IEEE Access
Multidisciplinary | Rapid Review | Open Access Journal

Received 20 March 2023, accepted 1 April 2023, date of publication 27 April 2023, date of current version 21 June 2023.

Digital Object Identifier 10.1109/ACCESS.2023.3270893

APPLIED RESEARCH

EMI Common-Mode Noise Suppression and Magnetic Elements Winding Loss Optimization Design Based on GaN Cascaded Power Module

GUOWANG LIU[1,2], MUXUAN XIAO[1], HONGLIN OUYANG[1], YINDA ZHU[1], AND BIN ZHANG[1], (Member, IEEE)

[1]College of Electrical and Information Engineering, Hunan University, Changsha 410012, China
[2]CRRC Zhuzhou Electric Locomotive Research Institute Company Ltd., Zhuzhou 412001, China

Corresponding author: Guowang Liu (278615320@qq.com)

This work was supported by the National Natural Science Foundation of China under Grant 51677063.

ABSTRACT In this paper, CM noise suppresion and magnetic elements winding loss optimization design of a cascade power module based on GaN design are carried out (the front stage is buck converter, the second stage is LLC resonant converter). To suppress CM noise, the front buck converter adopts planar stagger reverse coupling inductance, by establishing reverse stagger coupling buck converter CM noise model and conduction path model, the equivalent capacitance can effectively reduced, thus further reducing CM noise current. A staggered winding structure is proposed for second stage LLC resonant converter, compared and calculated LLC resonant transformer winding electromagnetic field characteristics with different structure. a novel shielding and cancellation technique is proposed for LLC resonant converter, by establishing LLC converter CM noise shielding model and the equivalent capacitance can effectively reduced, thus further reducing CM noise current. In order to improve the LLC resonant converter efficiency, winding copper foil optimal thickness is proposed. Experimental results show that power module with winding optimization and shielding technology can effectively suppress the CM noise and improve efficiency, CM noise can reduced 12-20dB, the peak efficiency improved about 1% after copper foil thickness is optimized.

INDEX TERMS Common-mode, reverse stagger winding structure, shielding technology, buck converter, LLC resonance converter.

I. INTRODUCTION

With the development of rail transit power electronic power converter towards high frequency, high efficiency and high power density, electromagnetic interference becoming more and more serious [7], [8]. EMI noise can divided into common-mode noise(CM)and differential mode noise(DM), common-mode noise is the most difficult EMC problem to deal with because of it's complicated conduction and radiation path [2], [3], [4], [5], [6]. The common-mode noise in frequency range of 150KHz-30MHz is conductive, in frequency range of 30MHz-1GHz is radiation. Common-mode conduction and radiation electromagnetic interference is mainly caused by the following reasons: ① Switching frequency increase: the fundamental and harmonic frequencies of the noise source increase with the increase of switching frequency [1], [2], [3]. ② Speed up switch: due to the distributed capacitance between potential changing switching device and zero potential ground conductor in the circuit, with the voltage of switching device V_{ds} jumping, the induced charge and pressure difference are formed, as the switching speed increases, the high frequency harmonic component of the noise source increases [5], [6], [7]. ③ Power density enhancement:with the increase of power density, the distance between magnetic devices decreases, magnetic leakage and coupling exist, and the near-field coupling between components strengthens [4]. In view of the environmentally friendly requirements of rail transit, EMI standards are increasingly strict [2]. Therefore, EMI common-mode noise is the most difficult problem to deal with in the design of high frequency

The associate editor coordinating the review of this manuscript and approving it for publication was Vitor Monteiro.

DC/DC power module [6], [7], [8].Traditional switching power EMI common-mode suppression strategies as follows: ① Reduce the number of potential jump points in the circuit from topological [5], [12], [13], [14]. ② Reducing the driving speed from the driving angle but with increase the switching loss as cost [9], [10], [11], [12]. ③ From PCB layout, reduce the high-frequency circuit, reduce the area of potential jump point to earth [3]. ④ From the angle of shielding, adopt shell shielding technology and device shielding technology. The LLC resonant converter in reference [3], [11] only use shielding technology to solve the EMI common-mode noise problem, and without use primary side winding and secondary side winding staggered technology to suppress *dv/dt* noise sources. In reference [13], EMI common-mode noise of buck converter is analyzed, but electromagnetic field modeling analysis and common-mode noise conduction path are not studied. Literature [8] has developed a cascaded power module with high switching frequency, as the two-stage voltage conversion architecture of the power module without adopt winding shielding technology, EMI common-mode noise can't meet the rail transit international EN 50155:2017 standards without additional conventional passive filters. Literature [19] only uses shielding technology, and magnetic field inside the transformer winding without use canceling technology, therefore, an extra filter needs to added at the power input to meet EMI standards. Considering high-efficiency and high-density power module PCB layout is mature enough and EMI common-mode noise cannot be improved by reducing the driving speed and sacrificing efficiency, this paper begins to optimize power module's EMI common-mode by improving circuit structure and transformer winding structure. power module's EMI common-mode performance optimized by buck converter interleaved coupling inductance winding structure and LLC transformer shielding technology, this method neither needs to pass additional conventional passive filters used for EMI mitigation, nor will affect efficiency of the system and sacrifice the volume of modules.

This paper uses *GaN* as switching device develop a cascade power module with high efficiency, high frequency and high power density. The first stage circuit architecture uses a two-phase interleaved buck converter convert the wide range voltage into a constant intermediate bus voltage (*48V*) through closed-loop control, buck converter switching frequency is 750kHz and then *LLC* resonant converter converts the intermediate bus voltage (*dc48V*) into a constant output voltage (dc24V) through open-loop control, *LLC* resonant converter switching frequency is about *1.5MHz*. In order to solve EMI common-mode noise caused by high frequency and high power density of cascaded power modules, power module coupling inductance interleaved winding technology, transform1er shielding technology and cancellation technology are studied and analyzed. In section II: a planar stagger coupling inductance is proposed for the front buck converter, adopted reverse stagger winding structure, establishing buck converter common-mode noise model and conduction path, buck converters inductance windings inter-layer structure capacitance under different winding structure were studied and compared, from buck converter noise source suppress common-mode noise and reduce the distributed capacitance to the ground. In section III: LLC resonant transformer common-mode noise suppression technology is studied and analyzed, proposed a secondary side noise shielding technique and cancellation technique, studied and compared LLC resonant transformer windings with different winding structure capacitance electric field characteristics and EMI effect, establishing LLC converter common-mode noise shielding model and conduction path. In section IV: in order to further improve the power module's density, LLC resonance transformer winding design is optimize, deduce LLC resonant converter winding loss mathematical model, the optimal copper foil design point of winding is obtained. In section V: develop two standard quarter brick power modules with the same voltage conversion architecture (buck and LLC): 1# power prototype buck and LLC converter adopts traditional winding structure. 2# power prototype buck converter rectifier inductance adopts reverse staggered coupling optimization structure, LLC resonant transformer adopts staggered winding structure and shielding technology. two power module's EMI common-mode noise, power loss and efficiency are compared and analyzed, through experimental analysis: power module optimized by staggered reverse winding technology and shielding technology EMI common-mode noise can reduced about 12-20dB, in the low frequency band, the maximum peak can drop 50dB, the winding adopts optimal copper foil design, the peak efficiency can be increased about 1%.

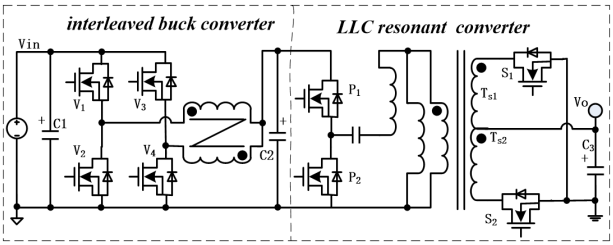

FIGURE 1. Power module topology architecture diagram.

Power module adopt above optimization design, all circuits are integrated in a standard quarter power brick module, the final prototype can reach 96.1% peak efficiency, the power density can reach 185W/in^3. the EMI performance of the optimized prototype can meet EN 50155:2017 standards without adding traditional filtering components. power module's topology shown as in fig.1.

II. EMC OPTIMIZATION DESIGN OF BUCK CONVERTER

Power module designed in this paper requires high efficiency, small volume and high power density, the EMI suppression strategy mentioned above can't realized by traditional buck converter without EMI filter. Buck converter EMI

common-mode noise suppression can only be implement from coupling inductance reverse winding optimization design.

A. ANALYSIS OF CM NOISE SOURCE OF TRADITIONAL DUAL-CHANNEL BUCK CONVERTER

In power module, two traditional buck converters are used for parallel conversion. Coupling structure is not used in the rectifier inductance [8]. The structure topology shown as fig.2:

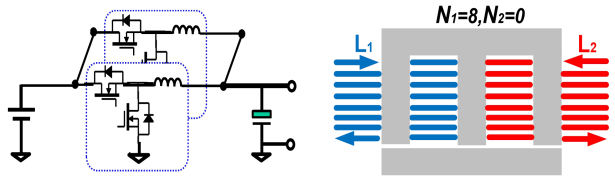

(a) without coupling inductance (b) winding no turn interleaved

FIGURE 2. Topology of dual buck converter and inductance winding structures.

Fig.3 shows the EMI common-mode noise model of dual-channel buck converter. the inductance of buck converter adopts planar inductance without coupling structure, capacitors C_a and C_b and resistors LISN form a Line Impedance Stable Network (LISN). C_a is the total distributed capacitance of A phase inductance to PGND, C_b is the total distributed capacitance of B phase inductance to PGND, the total distributed capacitance consists two parts: ① the capacitance between the switch tube and the heat sink. ② the capacitance between the heat sink and the PGND.

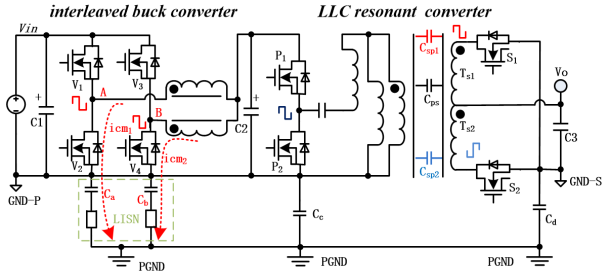

FIGURE 3. EMI model of CM noise in dual-channel buck converter.

The potential point A and point B in the circuit jumps with the opening and closing of switching tube V_2 and V_4 (dv/dt is generated). common-mode noise currents icm_1 and icm_2 are generated through corresponding distributed capacitors C_a and C_b respectively. Since u_A and u_B have the same phase, icm_1 and icm_2 common-mode noise currents are superimposed in phase.

$$\begin{cases} i_{cm1} = C_a du_a/dt \\ i_{cm2} = C_b du_b/dt \end{cases} \tag{1}$$

For a more intuitive understanding, the distributed capacitance of the buck converter is deeply analyzed. The calculation model of the inductance winding distributed capacitance is established, as shown in fig 4:

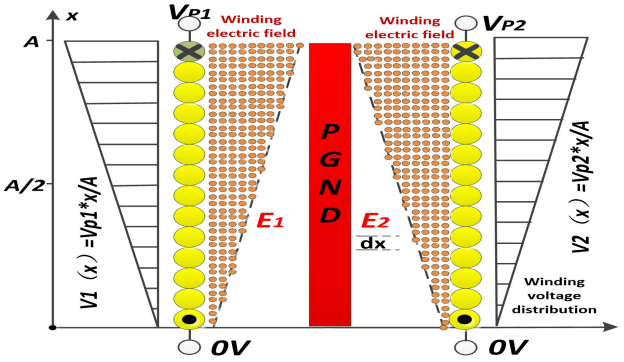

FIGURE 4. Winding potential distribution diagram without coupled structure.

In buck converter, the potential distribution between each turn winding of planar integrated inductance is not a fixed value, but is a certain potential gradient distribution. The effective port capacitance(EPC) that reflects the electric field energy stored in the winding is used for description and analysis. Since the flux through each turn of the winding is basically the same as the induced electromotive force, and the ac resistance of each turn of the winding is far less than the excitation inductance, the potential of the coil is considered to be linear distribution along the number of turns of the winding, and the effective capacitance of the port can be calculated by the method of electric field energy.

The following equation can be obtained from fig.4:

$$\begin{cases} V_{p1} = V_{p2} \\ \Delta V_1(x) = V_{p1} \cdot x/A \\ \Delta V_2(x) = V_{p2} \cdot x/A \end{cases} \tag{2}$$

C_0 is the total distributed structure capacitance, C is the winding unit structure capacitance, and $C=C_0/A$, the electric field energy stored in the planar inductance is:

$$\begin{aligned} E_{EPC1} = E_1 + E_2 &= \int_0^A \frac{1}{2} \cdot dC \cdot [V_1(x) + V_2(x)]^2 \\ &= \int_0^A \frac{1}{2} \cdot (\frac{C_0}{A}) \cdot dx \cdot 4 \cdot \Delta V_1(x)^2 = \frac{1}{2} \cdot (\frac{4C_0}{3}) \cdot V_P^2 \end{aligned} \tag{3}$$

The effective port capacitance of the planar integrated inductance is:

$$EPC_1 = \frac{4C_0}{3} \tag{4}$$

The CM noise current $\Delta i_{cm}(x)$ through the rectifier inductance winding with a length Δx express follow:

$$\begin{aligned} \Delta i_{cm-1}(x) &= \Delta i_{cm1}(x) + \Delta i_{cm2}(x) \\ &= EPC_1 * [V_1(x) + V_2(x)] \end{aligned} \tag{5}$$

The total current of port common-mode noise can be obtained through coupling superposition, as shown in

the following formula:

$$i_{cm-1} = \sum_0^A \Delta i_{cm}(x) = \int_0^A EPC_1 * [V_1(x) + V_2(x)] = \frac{4C_0V_P}{3} \tag{6}$$

B. OPTIMIZATION ANALYSIS OF CM NOISE SOURCE OF STAGGER BUCK CONVERTER

The power module designed in this paper can't suppress EMI noise from the topological structure and driving. It's only optimize design from the winding of the buck converter planar inductance, so introduce a reverse winding planar coupling inductance to cancel the common-mode noise of the reverse winding and suppress the common-mode noise of the buck converter from the source. The topology of the staggered buck converter and the planar reverse winding coupled inductance structure shown fig.5:

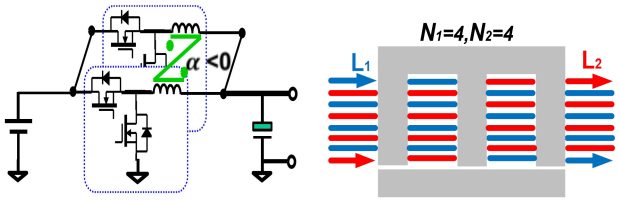

(a) coupling inductance (b) winding four turn interleaved

FIGURE 5. Stagger buck converter planar coupling inductance.

The top view and side view of the cross-coupling inductance core are shown in fig.6: W_1 and W_0 are length and width of the outside column respectively, W_w is the winding width, W_m is the middle column width; L, W and H are coupling inductance's length, width and height. W_2 is the inductance's length to width core ratio, Aw is the magnetic core cross-sectional, V_2 and V_1 are the core volume of the central column and outside column respectively [1].

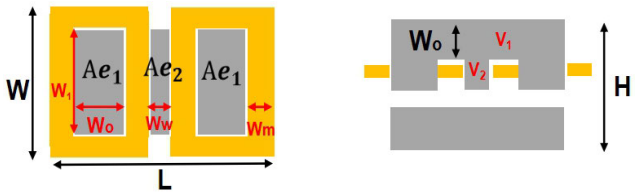

(a) Top view (b) Side view

FIGURE 6. Top view and side view of the coupling inductance core.

Fig.7 show the EMI common-mode noise model of stagger buck converter, the planar coupling inductance of buck converter adopts reverse winding structure. In normal operation, the amplitude of u_A and u_B is equal and the phase is opposite, so the common-mode noise current icm_1 is in the opposite direction to icm_2, which can achieve reverse cancellation from the noise source.

According to buck converter planar-coupled inductance reverse winding structure, establishing planar-coupled inductance winding distributed capacitance calculation model.

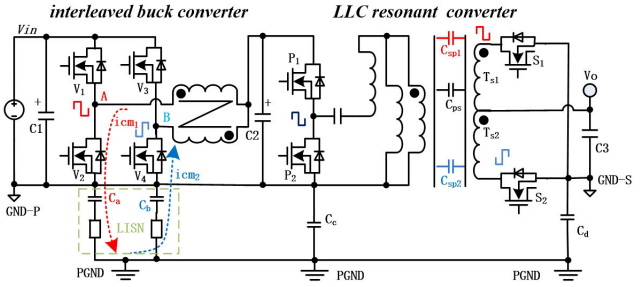

FIGURE 7. Electromagnetic interference model of CM noise in stagger buck converter.

The stagger buck converters planar coupling inductorance distributed capacitance are basically equal in magnitude and opposite in direction. According to the voltage distribution structure of the coupled inductance winding, calculate the electric field distribution between the inductance windings, and the electric field energy stored in the planar coupled inductance can be obtained by integration.

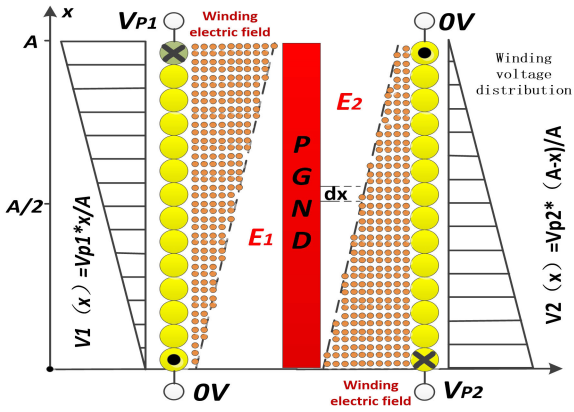

FIGURE 8. Structure potential distribution diagram of stagger buck coupling inductance winding.

According to fig.8: the voltage structure distribution of each winding can be deduced:

$$\begin{cases} V_{p1} = V_{p2} \\ \Delta V_1(x) = V_{p1} \cdot x / A \\ \Delta V_2(x) = V_{p2} \cdot (A - x) / A \end{cases} \tag{7}$$

The electric field energy stored in the planar-coupled inductance of the stagger buck converter is:

$$E_{EPC2} = E_1 - E_2 = \int_0^A \frac{1}{2} \cdot dC \cdot [V_1(x) - V_2(x)]^2 = \int_0^A \frac{1}{2} \cdot \left(\frac{C_0}{A}\right) \cdot dx \frac{(A - 2X)^2}{A^2} = \frac{1}{2} \cdot (\frac{C_0}{3}) \cdot V_P^2 \tag{8}$$

The equivalent capacitance of the planar integrated coupling inductor is:

$$EPC_2 = \frac{C_0}{3} \tag{9}$$

The CM noise current $\Delta i_{cm}(x)$ through planar coupling inductorance winding with a length Δx is expressed in

$$\begin{aligned}\Delta i_{cm-2}(x) &= |\Delta i_{cm1}(x) - \Delta i_{cm2}(x)| \\ &= EPC_2 * |V_1(x) - V_2(x)| \end{aligned} \tag{10}$$

The total current of port common-mode noise can be obtained through coupling superposition, as shown in the following formula:

$$\begin{aligned} i_{cm-2} &= \sum_0^A \Delta i_{cm}(x) = \int_0^A EPC_2 * |V_1(x) - |V_2(x)| \\ &= \int_0^{\frac{A}{2}} EPC_2 * [V_1(x) - V_2(x)] \\ &+ \int_{\frac{A}{2}}^A EPC_2 * [V_2(x) - V_1(x)] = \frac{C_0 V_P}{6} \end{aligned} \tag{11}$$

C. COMPARISON AND EXPERIMENTAL VERIFICATION ANALYSIS

Compare equations (4) and (9): buck converter rectifier inductance using reverse stagger coupled winding structure, planar inductance effective port capacitance can be reduced from $4C_0/3$ to $C_0/3$. compare equations (6) and (11): CM noise current can be effectively reduced from $4C_0V_P/3$ to $C_0V_P/6$, the CM current noise is separated by Fourier transform, as shown in equation 12: T_{dead} is the dead time, i_{cm-mag} is the magnitude of common-mode noise current during dead time.

$$\begin{aligned} i_{CM-T}(t) = i_{cm-mag} \cdot \frac{4T_{dead}}{T_S} \cdot \sum_{n=1,3,5...}^{\infty} \frac{\sin\left(n \cdot \pi \cdot \frac{T_{dead}}{T_S}\right)}{n \cdot \pi \cdot \frac{T_{dead}}{T_S}} \\ \cdot \sin\left(\frac{2n \cdot \pi}{T_S} t\right) \end{aligned} \tag{12}$$

LISN can be used to extract CM noise voltage and calculate EMI spectrum, as detailed in equation 13:

$$V_{CM-T}(t) = i_{CM-T}(t) \cdot R_{LSIN} \tag{13}$$

In order to verify buck converter reverse winding technology on common-mode noise suppression, the common-mode noise based on dual-path buck converter prototype (without coupled reverse winding technology) and stagger buck converter prototype of planar coupled inductor reverse winding were verified respectively, no filter was used during the test, the test results shown in fig 9:

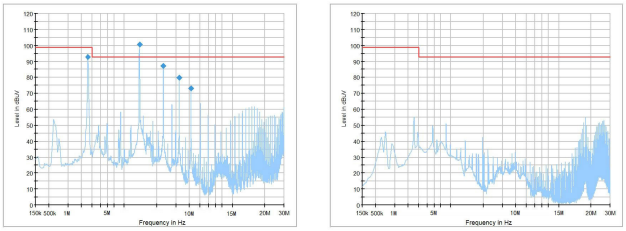

（a）without coupling structure　（b）with coupling structure

FIGURE 9. Comparison test of common-mode noise of two prototypes.

Through experimental analysis: buck converter planar coupling inductance with reverse staggered winding prototype's common-mode noise decreases about 15dB average in the range of 150K-30MHz compared with traditional buck converter. The common-mode noise of the traditional buck converter without coupled reverse winding technology has five deterioration peak point. Planar coupled inductance reverse winding technology can effectively suppress common-mode noise in the range of 150K-30MHz frequency band.

III. OPTIMIZATION OF EMC DESIGN FOR LLC RESONANT CONVERTER

In this paper, the second stage adopts LLC resonant converter convert the intermediate bus DC48V into DC24V constant output. using open loop control mode, switching device duty cycle is constant 50%, the common-mode noise model and conduction path of different windings (traditional winding structure and staggered winding structure) of LLC resonant converter are studied and compared. A winding shielding technique is proposed, the distributed capacitance of the primary and secondary sides of LLC resonant transformer is modeled and calculated, through experiment show: staggered winding and shielding technology can effectively reduce the equivalent capacitance of LLC resonant transformer and suppress the common-mode noise of LLC resonant converter from the source.

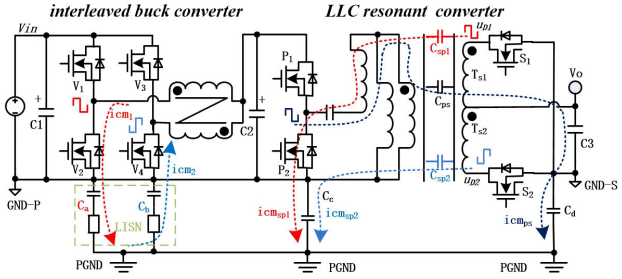

FIGURE 10. LLC resonant converter common-mode noise transmission path.

A. CM NOISE PATH AND MODEL ANALYSIS OF TRADITIONAL LLC RESONANT CONVERTER

The common-mode noise conduction path of traditional LLC resonant converter is shown fig.10: C_{ps} is the distribution capacitance of the primary side potential jump point to the secondary side winding, and C_{sp1} and C_{sp2} are the distribution capacitance of the secondary side potential jump point to the primary side winding.

The simplified common-mode noise model of LLC resonant converter is shown in fig 11: u_{D1} and u_{D2} have equal amplitude and opposite phase, and the generated common-mode noise current I_{CM1} is opposite to I_{CM2} phase.

LLC resonance transformer internal electric field characteristics shown fig.12: transformer primary side and secondary side don't adopt staggered winding structure, the common-mode noise current flowing through the distributed

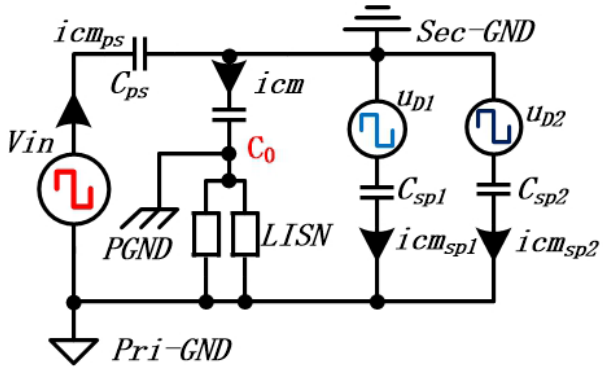

FIGURE 11. Simplified model of common-mode noise transmission for LLC resonant converter.

capacitors C_{sp1} and C_{sp2} is equal and opposite, so the common-mode noise can be cancelled.

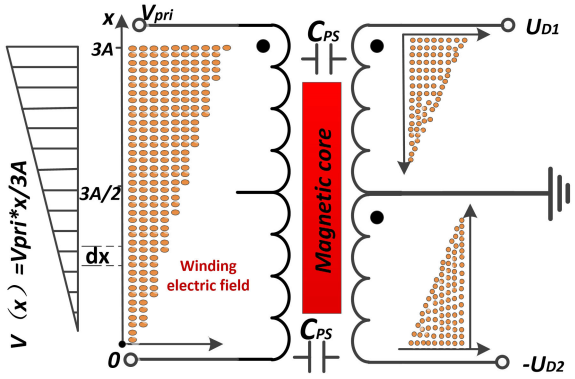

FIGURE 12. LLC resonance transformer internal electric field characteristics.

Fig.13 shows the equivalent capacitance distribution of winding of traditional LLC resonant transformer.

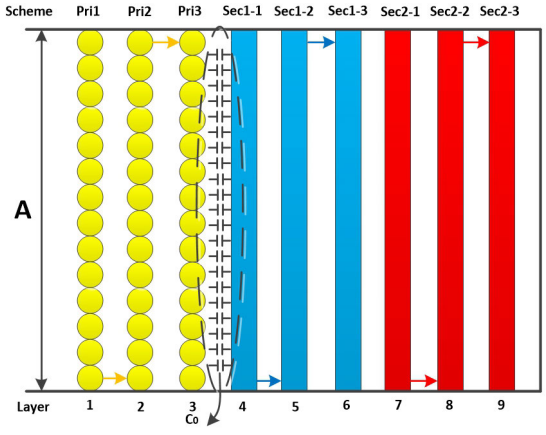

FIGURE 13. Analysis of electric field characteristics of winding of traditional LLC resonant transformer.

C_0 is the interlayer structure capacitance of winding, C is the winding unit capacitance structure capacitance, and C=3C$_0$/A, EPC$_{C0}$ is equivalent capacitance between winding layers, the amount of charge stored in the transformer is:

$$Q_1 = \int_0^{3A} \frac{3C_0}{A} \cdot \frac{u_{pri}x}{A} dx = \frac{3}{2} u_{pri} C_0 \tag{14}$$

Common-mode port effective capacitance is:

$$EPC_{C0} = \frac{Q_1}{u_{pri}} == \frac{3}{2} C_0 \tag{15}$$

The CM noise current $\Delta i_{cm1}(x)$ through the primary winding at position with a length Δx express follow:

$$\Delta i_{cm-llc-1}(x) = EPC_{C0} * V(x) \tag{16}$$

The total current of port common-mode noise can be obtained through coupling superposition, as shown in the following formula:

$$i_{cm-llc-1} = \int_0^{3A} EPC_{C0} * V(x) = \frac{9C_0 u_{pri}}{4} \tag{17}$$

B. LLC RESONANT CONVERTER WINDING OPTIMIZATION DESIGN AND SHIELDING TECHNOLOGY RESEARCH

LLC planar transformer adopts *EI* magnetic core design, the magnetic core is buckled on the *PCB*surface, *LLC* transformer engineering mass production can ensure the consistency of products. As shown in fig.14, r is the radius of the core and c is the width of the winding.

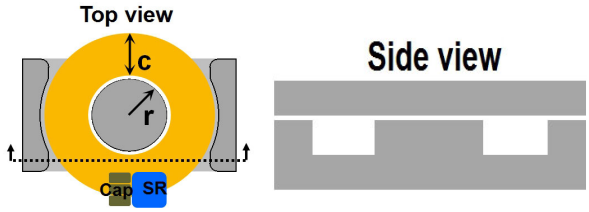

(a) top view (b) side view

FIGURE 14. Top view and side view of LLC transformer core.

In the design LLC resonant planar transformer, shielding structure is introduced between primary and secondary windings to realize secondary common-mode noise source shielding offset, the winding of transformer adopts staggered winding structure. staggered winding structure and shield cancellation technology resonant converter's common-mode noise conduction path as shown fig.15:

The simplified model of common-mode noise of LLC resonant converter using staggered winding structure and shielding cancellation technology is shown fig16: regardless of tolerance design error caused by process consistency, if C_{sp1} is equal to C_{sp2}, icm_{sp1} and icm_{sp2} caused by potential jump of transformer secondary side can also be cancelled.

LLC resonance transformer primary side and secondary side adopt staggered winding and shielding technology, transformer internal electric field characteristics as shown in fig 17:

Due to transformer inside primary and secondary side windings adopts staggered winding structure, there are many

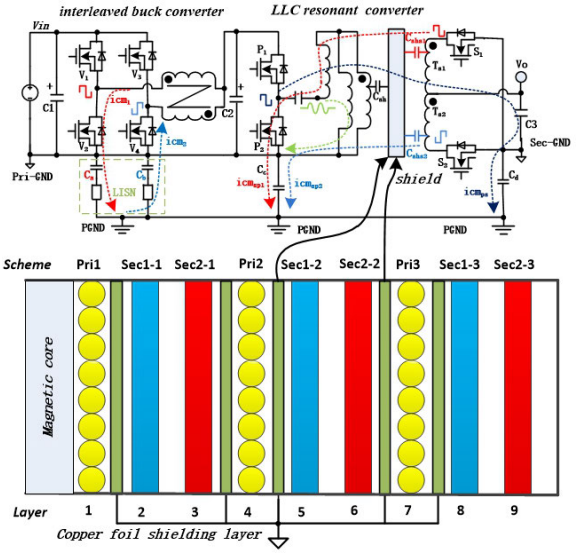

FIGURE 15. LLC resonant converter winding shielding technology common-mode noise transmission path.

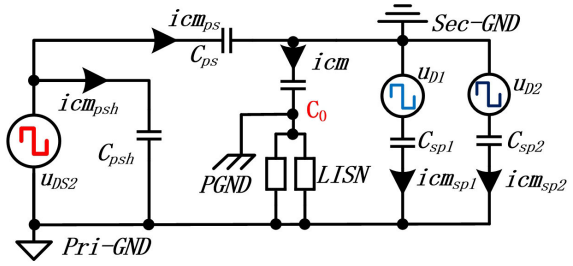

FIGURE 16. LLC resonant converter winding shielding technology common-mode noise simplified model.

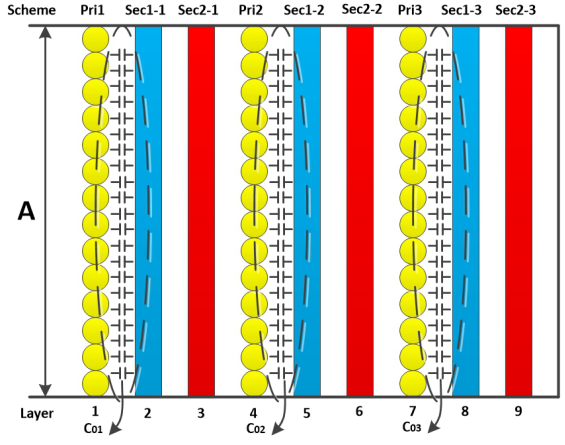

FIGURE 17. Electric field characteristic analysis diagram of LLC resonant transformer winding with staggered structure.

potential jump points inside the transformer, multiple electric fields and distributed capacitance in primary and secondary windings.

The electric field energy between the first layer winding of the primary side and the secondary side winding is:

$$Q_{01} = \int_0^A \frac{C_0}{A} u_{pri} \frac{x}{A} dx = \frac{u_{pri} C_0}{2} \tag{18}$$

The effective capacitance of the first layer winding of the primary side and the secondary side winding is:

$$EPC_{01} = \frac{Q_{01}}{u_{pri}} == \frac{C_0}{2} \tag{19}$$

The CM noise current through the first layer primary winding at position with a length Δx express follow:

$$\Delta i_{cm-llc-2(1)}(x) = EPC_{01} * \frac{u_{pri} x}{A} \tag{20}$$

The total current of common-mode noise of the port at the first layer of primary side winding can be obtained through coupling superposition, as shown in the following formula:

$$\begin{aligned} i_{cm-llc-2(1)} &= \sum_0^A \Delta i_{cm-llc-2(1)}(x) \\ &= \int_0^A EPC_{01} * \frac{u_{pri} x}{A} = \frac{C_0 u_{pri}}{4} \end{aligned} \tag{21}$$

The electric field energy between the second layer winding of the primary side and the secondary side winding is:

$$Q_{02} = \int_0^A \frac{C_0}{A} \cdot (\frac{2 \cdot u_{pri}}{3} \cdot \frac{x}{A}) dx = \frac{u_{pri} C_0}{3} \tag{22}$$

The effective capacitance of the second layer winding of the primary side and the secondary side winding is:

$$EPC_{02} = \frac{Q_{02}}{u_{pri}} == \frac{C_0}{3} \tag{23}$$

The CM noise current through the primary winding second layer at position with a length Δx express follow:

$$\Delta i_{cm-llc-2(2)}(x) = EPC_{02} * \frac{2 u_{pri} x}{3A} \tag{24}$$

The total current of common-mode noise of the port at the second layer of primary side winding can be obtained through coupling superposition, as shown in the following formula:

$$\begin{aligned} i_{cm-llc-2(2)} &= \sum_0^A \Delta i_{cm-llc-2(2)}(x) = \int_0^A EPC_{02} * \frac{2 u_{pri} x}{3A} \\ &= \frac{C_0 u_{pri}}{6} \end{aligned} \tag{25}$$

The electric field energy between the third layer winding of primary side and secondary side winding is:

$$Q_{03} = \int_0^A \frac{C_0}{A} \cdot (\frac{u_{pri}}{3} \cdot \frac{x}{A}) dx = \frac{u_{pri} C_0}{6} \tag{26}$$

The effective capacitance of the third layer winding of the primary side and the secondary side winding is:

$$EPC_{03} = \frac{Q_{03}}{u_{pri}} == \frac{C_0}{6} \tag{27}$$

The CM noise current through the primary winding third layer at position with a length Δx express follow:

$$\Delta i_{cm-llc-2(3)}(x) = EPC_{03} * \frac{u_{pri}x}{3A} \tag{28}$$

The total current of common-mode noise of the port at the third layer of primary side winding can be obtained through coupling superposition, as shown following formula:

$$i_{cm-llc-2(3)} = \sum_0^A \Delta i_{cm-llc-2(3)}(x) = \int_0^A EPC_{03} * \frac{u_{pri}x}{3A} = \frac{C_0 u_{pri}}{9} \tag{29}$$

The total effective capacitance of common-mode port of LLC resonant transformer is:

$$EPC_{C1} = C_{01} + C_{02} + C_{03} = C_0 \tag{30}$$

In the above formula, C_{01}, C_{02} and C_{03} is the transformer's internal structure capacitance. LLC resonant converter common-mode noise total current is:

$$i_{cm-llc-2} = \sum_1^3 i_{cm-llc-2(x)} = \frac{19C_0 u_{pri}}{36} \tag{31}$$

C. COMPARISON AND EXPERIMENTAL VERIFICATION ANALYSIS

Compare equations (15) and (30): LLC resonant transformers by using winding staggered structure and shielding technology, effective port capacitance can be reduced from $3C_0/2$ to C_0. reference equations (17) and (31): CM noise current can be effectively reduced from $9C_0 u_{\mathrm{Pr}i}/4$ to $19C_0 u_{\mathrm{Pr}i}/36$.

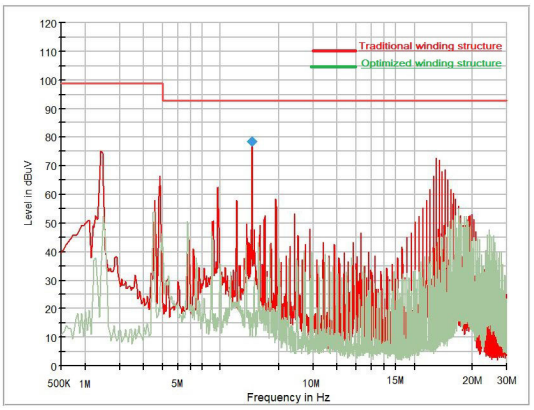

FIGURE 18. Common mode noise comparison test results.

In fig. 18, the green test curve is the common-mode conduction noise of the resonant converter with staggered winding structure and shielding technology. the red test curve is the common-mode conduction noise of traditional winding structure. through experiments analysis: the common-mode noise of LLC resonant converter based on taggered winding and shield technology can decrease 10dB than LLC resonant converter based on traditional winding ethod (without shielding technology) in the range of 150K-30MHz. the common-mode noise of LLC resonant converter prototype designed by traditional winding method has deterioration peak point at 1.5MHz.

IV. OPTIMIZATION DESIGN OF WINDING LOSS OF PLANAR PCB MAGNETIC ELEMENT

In this chapter, LLC resonant converter winding loss is studied and analyzed. Reducing magnetic components winding loss includes following aspects: the design can optimized from reduce the winding window magnetic field intensity distribution. select the conductance wire diameter with minimum winding loss, and an appropriate number of turns can designed to optimize the total loss of core devices. Due to the use of planar magnetic core design, and using compact 1/4 standard brick structure, the transformer winding loss can't optimized from reducing the winding window's magnetic field intensity, but can optimized from power modules magnetic component copper foil thickness.

LLC transformer secondary winding adopts center tap mode, designed into a perfect staggered structure. Transformer winding structure has been shown in fig 15: priI-secI-secII staggered distribution structure, *LLC* resonance transformer turns ratio is priI-secI-secII = 3:3:3. *LLC* planar transformer adopts *EI* magnetic core design, the magnetic core is buckled on the *PCB*surface. $k(f_s) = \sqrt{j2\pi f_s \sigma \mu}$, f_s is the switching frequency, μ is the permeability.

Magnetic field distribution in winding:

$$H(\mathrm{x}, f_s, W_w, H_{1x}, H_{2x}) = \frac{H_{1\mathrm{x}} * \sinh[k(f_s) * (W_w - x)] + H_{2\mathrm{x}} * \sinh[k(f_s) * x]}{\sinh(k(f_s) * W_w)} \tag{32}$$

The electric field distribution in winding:

$$J(\mathrm{x}, f_s, W_w, H_{1x}, H_{2x}) = kk(f_s) * \frac{[H_{1\mathrm{x}} * \sinh(k(f_s) * (W_w - x)) + H_{2\mathrm{x}} * \sinh(k(f_s) * x)]}{\sinh(k(f_s) * W_w)} \tag{33}$$

Winding ac loss show in fig 17:

$$P_{\mathrm{ac}}(f_s, W_w, H_{1x}, H_{2x}) = \frac{1}{2\sigma} \int_0^{W_w} J(\mathrm{x}, \mathrm{fx}, W\mathrm{w}, H1\mathrm{x}, H2\mathrm{x})^2 dx \tag{34}$$

Winding dc loss:

$$P_{\mathrm{dc}}(W_w, J_{\mathrm{dc}x}) = \frac{J_{\mathrm{dc}x}^2}{W_{\mathrm{w}}\sigma} \tag{35}$$

J_{dcx} is the dc current density in the direction of altitude; P_{ac} and P_{dc} are the unit loss in the direction of height.

Calculate the ac and dc losses of each harmonic in each conductor layer.

$$\begin{cases} Pac\_layer(layer, Ww) \\ \quad = \sum_{k=1}^{Nharm} A * Pac(k * f_s, Ww, H_{1k,lawer}, H_{2k,lawer}) \\ \mathrm{Pdc}\_layer(layer, Ww) = A * Pdc(Ww, Jdc_{lawer}) \end{cases} \tag{36}$$

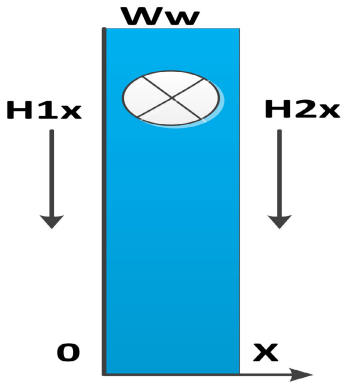

FIGURE 19. Magnetic field density per unit length of winding.

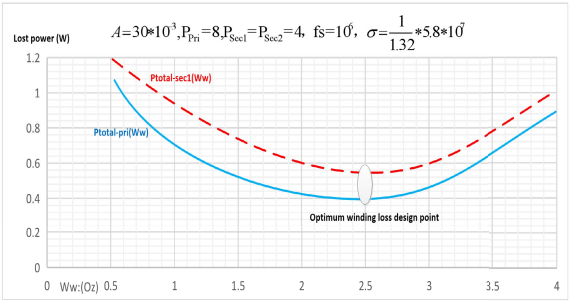

FIGURE 20. LLC resonance transformer winding loss VS copper thickness curve.

The total loss of primary and secondary winding, as in (37), shown at the bottom of the page.

According to mathematical model of primary side loss and secondary side loss, the copper thickness and loss curve of winding can obtained. The winding's copper thickness is 2.5 oz, the winding loss is optimal, as shown fig.20:

In this chapter, established LLC planar transformer winding loss model, the magnetic field density distribution and current density distribution of planar transformer winding are modeled and calculated accurately. AC and DC losses of each harmonic are analyzed iterally, according to the total loss analysis results selected the optimal copper foil thickness.

V. EXPERIMENTAL VERIFICATION ANALYSIS

A. DESIGN PARAMETERS AND PROTOTYPE COMPARATIVE ANALYSIS

This paper designs two power modules prototype with the same topology, both power modules adopt two-stage topology transformation architecture(buck and LLC). The size of the two power module is compatible with the standard package (*2.3 inch x 1.45 inch*). main power switch tube, inductance core, LLC transformer core and switching frequency of the two power modules are consistent. only difference lies in buck converter inductance winding structure and LLC resonant transformer winding structure.

1# power prototype: buck converter rectifier inductance adopts traditional winding scheme without reverse cross-coupling structure. LLC resonance transformer adopts traditional winding structure. power module all windings adopt traditional 2 oz copper thickness, the maximum output power is 200W. 2# power prototype: buck converter rectifier inductance adopts reverse staggered coupling optimization structure. LLC resonant transformer adopts staggered winding structure, primary and secondary winding adopts shielding technology. power module all windings adopt 2.5 oz copper thickness, the maximum output power is 200W consistent. Both power modules key parameters designed in this paper are shown in table 1.

TABLE 1. Key parameters of the power module in this paper.

buck	input voltage	DC60-160V
	output voltage	DC48V
	Working frequency	750KHz
	Switching devices	GS66506T
	Coupling inductance self induction	10uH
LLC	input voltage	DC48V
	output voltage	DC24V
	Working frequency	1.5MHz
	Switching devices	EPC2029
	resonant capacitance	1200nF
	Magnetizing inductance	750nH
	resonant inductance	80nH

Key parameters of the power module in this paper

B. COMPARATIVE ANALYSIS OF PROTOTYPE LOSS AND EFFICIENCY

Two power module's thermal imaging experiments comparison and analysis as shown in fig 23: under the condition of rated input voltage and full load output, the temperature rise of the buck converter and LLC resonant converter in the power module can be reduced average 10° after the winding optimization.

$$\begin{cases} P_{total\_\mathrm{pri}}(Ww) = \sum_{layer\_k=3}^{4} [Pac\_layer(lay\,\mathrm{ker}, Ww) + Pdc\_layer(lay\,\mathrm{ker}, Ww)] \\ P_{total\_\mathrm{sec}}(Ww) \\ = \sum_{layer\_k=1}^{2} [Pac\_layer(lay\,\mathrm{ker}, Ww) + Pdc\_layer(lay\,\mathrm{ker}, Ww)] \\ + \sum_{layer\_k=5}^{6} [Pac\_layer(lay\,\mathrm{ker}, Ww) + Pdc\_layer(lay\,\mathrm{ker}, Ww)] \end{cases} \tag{37}$$

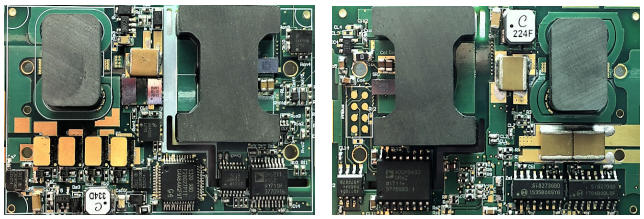

FIGURE 21. Power module without coupling structure top and bottom view.

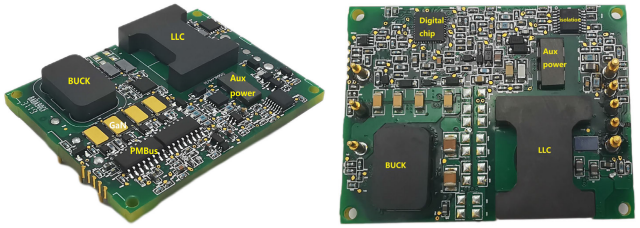

FIGURE 22. Power module with coupling structure top and bottom view.

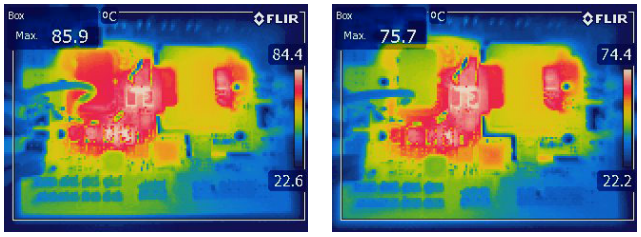

(a) 1# without coupling structure (b) 2# with coupling structure

FIGURE 23. Comparative analysis of prototype at full load thermal imaging.

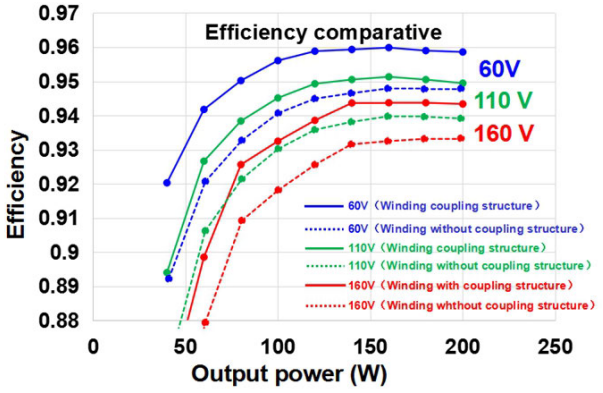

FIGURE 24. The efficiency curve and comparative analysis diagram.

Compare and test the efficiency of two power modules in fig.22: in the whole input voltage range, power module's efficiency with winding optimized design and shielding technology is 1% higher than before optimization.

C. COMPARATIVE ANALYSIS OF POWER MODULES CONDUCTION TEST

In order to verify the EMC interference performance of the two power modules, a comparative test of EMC conducted noise was conducted, including full-load output at different input voltages (DC60V,DC110V,DC160V), as shown in fig 25: CM noise test bench include impedance load, power module, linear impedance stabilization network and EMI fully automatic test receiver. the conducting common-mode noise of the 2# power module with optimized winding is green, the conducting common-mode noise of 1# power module without optimized winding is blue.

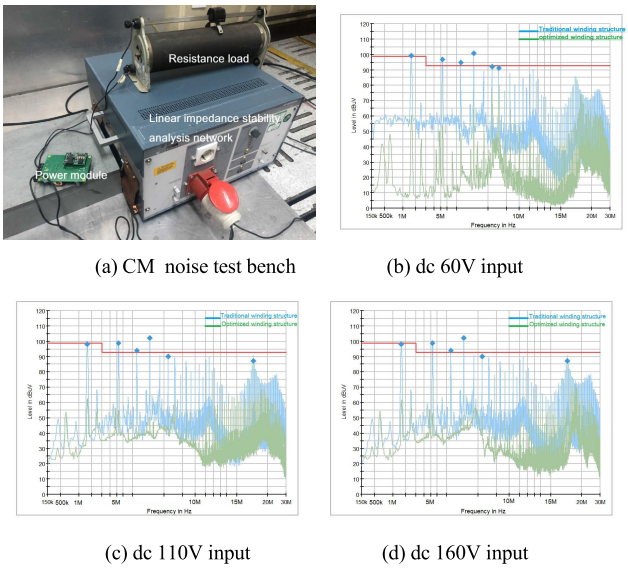

(a) CM noise test bench (b) dc 60V input

(c) dc 110V input (d) dc 160V input

FIGURE 25. Comparative analysis diagram of conducted common-mode noise.

Experimental results show that the conduction noise can effectively reduced within the full input voltage range by optimizing power module internal buck converter rectifier inductance and LLC resonant transformer winding structure. In particular, common-mode noise suppression is superior under low voltage input conditions. Power module with winding optimization design conduction common-mode noise can decreases about 12-20dB in the range of 3MHz-30MHz compared with traditional power module without optimization. the maximum common-mode noise can be reduced more than 50dB especially in the low frequency part.

VI. CONCLUSION

In this paper, the common-mode noise and efficiency of the cascaded power module (the front stage is buck converter, and the second stage is LLC resonant converter) are studied and analyzed. In order to solve the EMI common-mode noise problem, the front buck converter in the power module adopts stagger direction coupling winding structure to reduce the port capacitance and effectively suppress the common-mode noise transmission path. second LLC resonant circuit of the power module adopts staggered winding structure and shielding technology, the common-mode noise conduction path and port equivalent capacitance model is established. In order to further reduce the power loss of the power module, the PCB planar magnetic components are studied and analyzed, LLC

resonant converter winding loss model is established, and the optimal design value of the winding copper foil is proposed. Two research prototypes (the traditional winding scheme and the optimized scheme in this paper) were developed for comparative analysis conducted common-mode noise and efficiency loss. The overall common-mode noise of the power module using staggered winding optimization and shielding technology can reduced about 12-20dB on average compared with the traditional scheme. LLC transformer windings with the copper foil optimal design, the power module winding's loss can be effectively improved, where the peak efficiency can increase up to 1%.

REFERENCES

[1] G. Liu, H. Ouyang, and M. Xiao, "Optimal design of high frequency high efficiency and high-power density DC–DC power module based on GaN," *IET Power Electron.*, vol. 2022, pp. 1–16, Aug. 2022.
[2] Y. Cao, Y. Chen, X. Huang, P. Ren, W. Chen, and X. Yang, "EMI noise reduction in GaN-based full-bridge LLC converter," in *Proc. IEEE Workshop Wide Bandgap Power Devices Appl. Asia (WiPDA Asia)*, Wuhan, China, Aug. 2021, pp. 276–280.
[3] Y. Zhang and D. Jiang, "An active EMI filter in grounding circuit for DC side CM EMI suppression in motor drive system," *IEEE Trans. Power Electron.*, vol. 37, no. 3, pp. 2983–2992, Mar. 2022.
[4] Y. Zhang, Q. Li, and D. Jiang, "A motor CM impedance based transformerless active EMI filter for DC-side common-mode EMI suppression in motor drive system," *IEEE Trans. Power Electron.*, vol. 35, no. 10, pp. 10238–10248, Mar. 2020.
[5] C. Yao, Z. Wang, W. Li, H. Li, J. Qian, C. Han, F. Luo, and J. Wang, "Comparison study of common-mode noise and thermal performance for lateral wire-bonded and vertically integrated high power diode modules," *IEEE Trans. Power Electron.*, vol. 33, no. 12, pp. 10572–10582, Dec. 2018.
[6] M. Asad, A. K. Singha, and R. M. S. Rao, "Dead time optimization in a GaN-based buck converter," *IEEE Trans. Power Electron.*, vol. 37, no. 3, pp. 2830–2844, Mar. 2022.
[7] L. Dai, W. Chen, X. Yang, M. Zheng, Y. Yang, and R. Wang, "A multifunction common mode choke based on active CM EMI filters for AC/DC power converters," *IEEE Access*, vol. 7, pp. 43534–43546, 2019.
[8] M. Fu, C. Fei, Y. Yang, Q. Li, and F. C. Lee, "Optimal design of planar magnetic components for a two-stage GaN-based DC–DC converter," *IEEE Trans. Power Electron.*, vol. 34, no. 4, pp. 3329–3338, Apr. 2019.
[9] S. Zhang and X. Wu, "Low common mode noise half-bridge LLC DC–DC converter with an asymmetric center tapped rectifier," *IEEE Trans. Power Electron.*, vol. 34, no. 2, pp. 1032–1037, Feb. 2019.
[10] K.-W. Kim, Y. Jeong, J.-S. Kim, and G.-W. Moon, "Low common-mode noise full-bridge LLC resonant converter with balanced resonant tank," *IEEE Trans. Power Electron.*, vol. 36, no. 4, pp. 4105–4115, Apr. 2021.
[11] D. Vanitha and M. Rathinakumar, "Current mode controlled PV based buck boost converter system using coupled inductor with reduced current ripple," in *Proc. 4th Int. Conf. Adv. Electr., Electron., Inf., Commun. Bio-Inform. (AEEICB)*, Feb. 2018, pp. 1–6.
[12] C. Seng, J. Seo, W. Kim, and H. Cha, "High-frequency equivalent circuit model for common-mode noise of buck converter," in *Proc. 24th Int. Conf. Electr. Mach. Syst. (ICEMS)*, Oct. 2021, pp. 228–231.
[13] P. B. Derkacz, P. Musznicki, and P. J. Chrzan, "EMI attenuation in a DC–DC buck converter using GaN HEMT," *IEEE J. Emerg. Sel. Topics Power Electron.*, vol. 9, no. 4, pp. 4146–4152, Aug. 2021.
[14] X. Huang, F. C. Lee, Q. Li, and W. Du, "High-frequency high-efficiency GaN-based interleaved CRM bidirectional buck/boost converter with inverse coupled inductor," *IEEE Trans. Power Electron.*, vol. 31, no. 6, pp. 4343–4352, Sep. 2016.
[15] O. Knecht, D. Bortis, and J. W. Kolar, "ZVS modulation scheme for reduced complexity clamp-switch TCM DC–DC boost converter," *IEEE Trans. Power Electron.*, vol. 33, no. 5, pp. 4204–4214, May 2018.
[16] C. Fei, Y. Yang, Q. Li, and F. C. Lee, "Shielding technique for planar matrix transformers to suppress common-mode EMI noise and improve efficiency," *IEEE Trans. Ind. Electron.*, vol. 65, no. 2, pp. 1263–1272, Feb. 2018.
[17] G. Liu, Y. Zhang, and L. Wang, "Research on the push-pull forward capacitor clamp zero-voltage synchronous rectifier converter," *Control Inf. Technol.*, no. 1, pp. 57–64, Feb. 2023.
[18] M. Tian, Y. Hao, K. Wang, Y. Xuan, L. Huang, J. Sun, and X. Yang, "EMI modeling and experiment of a GaN based LLC half-bridge converter," in *Proc. 9th Int. Conf. Power Electron. ECCE Asia*, Jun. 2015, pp. 1961–1966.
[19] J. Sun, W. Chen, and X. Yang, "EMI prediction and filter design for MHz GaN based LLC half-bridge converter," in *Proc. IEEE 8th Int. Power Electron. Motion Control Conf.*, Hefei, China, May 2016, pp. 297–304.

GUOWANG LIU was born in Loudi, Hunan, China. He is currently pursuing the Ph.D. degree in energy power engineering with Hunan University, China. Since 2014, he has been a Senior Researcher of power converter technology with CRRC Zhuzhou Electric Locomotive Research Institute. His research interests include switching power supplies for rail transit, power modules, the applications of wide-band gap devices in power converters, and high-efficiency magnetic designs.

MUXUAN XIAO was born in Hunan, China, in 1989. He received the M.S. and Ph.D. degrees in electrical engineering from Hunan University, Changsha, China, in 2014 and 2021, respectively. He is currently doing a post Ph.D. research in electrical engineering with Hunan University. His research interests include dc/dc converters, motor driver, and multilevel converters.

HONGLIN OUYANG was born in Qidong, Hunan, China, in January 1965. He received the Ph.D. degree in engineering from the School of Electrical and Information Engineering, Hunan University, China, in June 2005. He is currently a Professor and a Doctoral Supervisor with the School of Electrical and Information Engineering, Hunan University. With scientific research ability to solve major projects in the field of electrical engineering, with high-attainments in the field of power electronics and control engineering.

YINDA ZHU, photograph and biography not available at the time of publication.

BIN ZHANG (Member, IEEE) was born in Hunan, China. He received the B.S. and M.S. degrees in electrical engineering from Northwestern Polytechnical University. He is currently pursuing the Ph.D. degree in electrical engineering with Hunan University, Changsha, China. His research interests include deep learning and power electronic.